Hindawi
Geofluids
Volume 2021, Article ID 6693131, 11 pages
https://doi.org/10.1155/2021/6693131

*Research Article*

# Investigation on Creep Behavior and Permeability Evolution Characteristics of Sandstone under Different Pore Pressures

**Hongcai Shi**

*Department of Civil Architecture and Environment, Hubei University of Technology, Wuhan, China 430068*

Correspondence should be addressed to Hongcai Shi; baoshi284117400@163.com

Received 2 December 2020; Revised 24 December 2020; Accepted 4 January 2021; Published 14 April 2021

Academic Editor: Zhigang Tao



To investigate the influence of pore pressure ($\sigma_w$) on the creep behavior and permeability of red sandstone, triaxial creep test with permeability test under different pore pressures was conducted using MTS 815 testing system. The experimental results demonstrate that water has significant weakening effect on the long-term mechanical properties of sandstone, and the long-term strength of sandstone gradually decreases with increase in pore pressures. All permeability-time curves demonstrate a "decreasing-increasing" trend, but two different permeability evolution trends during the steady creep stage are observed, which are related to deviatoric stress. The permeability of both intact ($k_0$) and fractured sandstone ($k_f$) samples increases with the increase in pore pressure, which are in consistent with the failure mode analysis of fractured sandstone samples. However, while the relationship between $k_0$ and $\sigma_w$ is positive linear, it is a positive exponential function relationship between $k_f$ and $\sigma_w$.

## 1. Introduction

Undersea tunnels and lake tunnels have drawn great attention in recent years since it is an optimal choice of overcoming geographical barriers [1–4]. In China, these tunnels are basically constructed in sandstone stratum, which is a common rock subbase in roadway, hydropower station, and mining engineering. Under the influence of groundwater, the mechanical properties of rock are deteriorated, thus decreasing the stability of rock formation and the safety of underwater tunnels [5–10]. Due to the influence of water-rock interaction, the surrounding rock and stratum is inclined to yield and destroy, thus increasing the risk of instability of tunnels and slopes [11, 12]. By investigating the short-term and long-term mechanical properties, the time-dependent deformation characteristics, reinforcement method, and support design of rock tunnels or foundations could be obtained [13–15]. Therefore, it is of great significance to study the creep behavior and permeability evolution characteristics of sandstone under different pore pressures.

Considerable investigations on the water effect on the engineering mechanical properties of rock have been conducted. Liu et al. [16] and Vásárhelyi et al. [17] conducted uniaxial compression tests on sandstone with different water contents, and the results indicated that the UCS (uniaxial compressive strength) of sandstone gradually decreases with the increase in water content. Similarly, Li et al. [18] and Chen et al. [19] had conducted triaxial compression tests on dry and saturated sandstone, and they concluded that both TCS (triaxial compressive strength) and elastic modulus of dry sandstone samples are larger than that of saturated sandstone. However, in rock engineering projects such as underground gas storage, tunnels, and hydropower station, understanding the long-term mechanical properties of rock is also important. Some researchers are interested in the water effects on the long-term mechanical behavior of sandstone. Yu et al. [20] and Tang et al. [21] carried out uniaxial compression creep tests on sandstone under dry and saturated conditions and pointed out that the creep deformation of quartz greywacke in saturated state is greater than that in dry state. Yang et al. [22] also conducted both triaxial compression and creep tests on sandstone under different pore pressures, and they proposed that while compression strength of sandstone decreased with increasing pore pressure, creep rate increased with the increase in pore pressure. However, previous studies hardly pointed out the

permeability evolution characteristics of surrounding rock under creep process, which is an important parameter to evaluate the long-term stability of underground engineering. Therefore, a compressive study on both the creep behavior and permeability evolution characteristics of rock under different pore pressures is needed to examine the long-term safety of sandstone under the influence of underground water, which is also the objective of this research.

To reveal the water-rock interaction effects on creep behavior and permeability evolution characteristics of sandstones, the triaxial creep tests of red sandstone under different pore pressures (i.e., 0 MPa, 2.5 MPa, 5 MPa, and 10 MPa) were carried out on MTS 815 rock mechanics testing system, and the permeability of sandstone under different conditions was tested in the whole process. Based on the experimental results, the creep behavior of sandstone under triaxial creep tests was analyzed, and the influence of pore pressure on mechanical properties was discussed. Finally, the permeability evolution characteristics of sandstone under different conditions were deeply analyzed along with the failure mode of sandstone samples.

## 2. Sample Preparation and Test Design

*2.1. Sample Preparation.* The red sandstone block was taken from a tunnel excavation project at the bottom of the Yangtze River at the depth of 100 m in Jiangsu Province, China. All cylindrical red samples were cored at the same direction from the rock block, and subsequently, they were finely fabricated into standard specimens with 50 mm in diameter and 100 mm in length, following the method recommended by ISRM [23]. Tested sandstone samples are intact with good integrity and no joints on the surface (Figure 1). The X-ray diffraction (XRD) analysis indicates that the mineral components of tested specimens are feldspar, quartz, kaolinite, calcite, and hematite (Figure 2). The average density of natural sandstone samples is 2.37 g/cm$^3$, and the average longitudinal wave velocity is 2424 m/s. The basic parameters and test conditions are listed in Table 1.

*2.2. Testing Apparatus.* All tests on sandstone specimens under HM coupling conditions were conducted on a MTS 815 testing machine at Hunan University of Science and Technology. The maximum axial loading capacity of the equipment is 4600 kN, the maximum confining pressure is 100 MPa, and the maximum hydraulic pressure is 20 MPa. The configuration of rock specimen installation with other sensors is shown in Figure 3 below. The axial deformation was measured by a pair of linear variable differential transformers (LVSTs) with a range of -5~5 mm. The control accuracy of the above equipment and sensors is within 5‰. The diagram of the whole testing system is shown in Figure 3.

*2.3. Testing Procedure.* All the specimens were saturated for 24 h in a vacuum saturation equipment before the triaxial compression (TC) test and multistage creep (MC) test. The triaxial compression tests at different pore pressures were conducted before creep tests at the confining pressure of 5 MPa. Figure 4 shows the stress-strain curves of red sandstone samples under triaxial compression tests, and the mechanical parameters obtained from stress-strain curves are listed in Table 2. Both triaxial compression strength (TCS) and Young modulus decrease with the increase in pore pressure, and the TCSs of red sandstone specimens at different pore pressures are 198.92 MPa, 180.81 MPa, 158.77 MPa, and 123.40 MPa, respectively. Therefore, the deviatoric stress

Figure 1: Red sandstone samples.

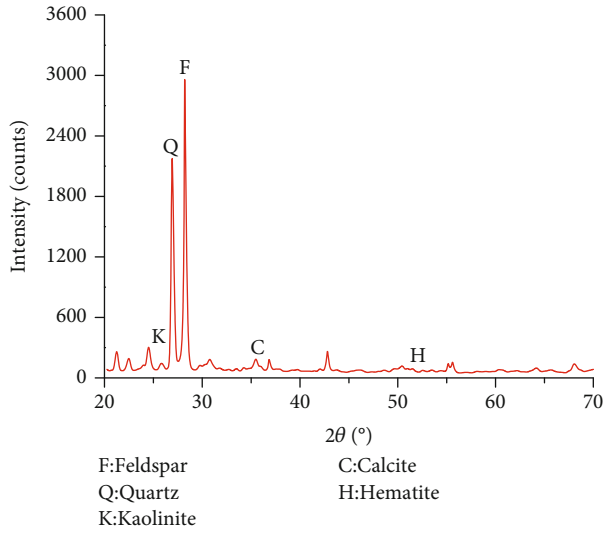


Figure 2: XRD analysis of red sandstone.

Table 1: Physical parameters and test conditions of red sandstone samples.

| Specimen | $L$/mm | $D$ /mm | $\rho$ /g·cm$^{-3}$ | $v_h$ /m·s$^{-1}$ | $\sigma_3$ /MPa | $\sigma_w$ /MPa | Testing design |
|---|---|---|---|---|---|---|---|
| HMS-1 | 101.32 | 50.65 | 2.35 | 2415 | 5 | 0 | TC |
| HMS-2 | 99.89 | 50.12 | 2.37 | 2424 | 5 | 2.5 | TC |
| HMS-3 | 98.76 | 50.11 | 2.42 | 2398 | 5 | 5 | TC |
| HMS-4 | 100.56 | 50.08 | 2.32 | 2451 | 5 | 10 | TC |
| HML-1 | 100.21 | 50.05 | 2.39 | 2432 | 5 | 0 | MC |
| HML-2 | 98.90 | 49.87 | 2.41 | 2441 | 5 | 2.5 | MC |
| HML-3 | 101.15 | 50.12 | 2.35 | 2409 | 5 | 5 | MC |
| HML-4 | 100.32 | 50.15 | 2.36 | 2425 | 5 | 10 | MC |

Notes: $L$ is length, $D$ is diameter, $\rho$ is density, $v_h$ is elastic wave velocity, $\sigma_3$ is confining pressure, and $\sigma_w$ is pore pressure.

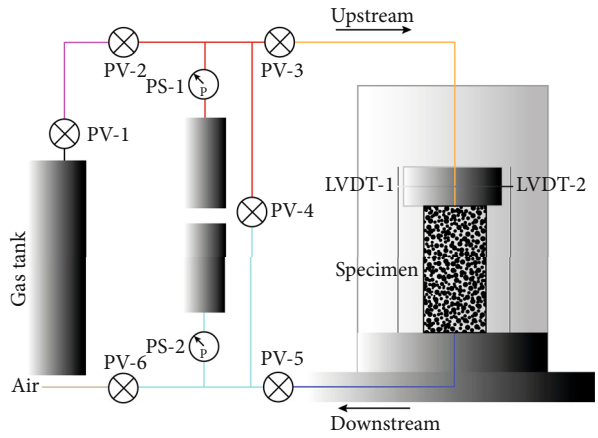


Figure 3: Testing equipment diagram.

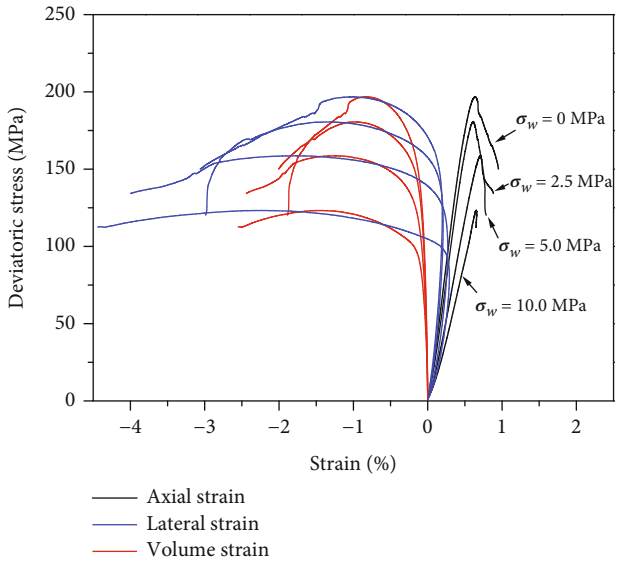


Figure 4: Stress-strain curves of sandstone samples under triaxial compression test.

Table 2: Mechanical parameters of red sandstone samples under different hydraulic pressures.

| Specimen | $\sigma_3$/MPa | $\sigma_w$/MPa | $\sigma_c$/MPa | $E_s$/GPa | $\varepsilon_{1c}/10^{-3}$ |
|---|---|---|---|---|---|
| HMC-1 | 196.92 | 0 | 198.92 | 37.63 | 6.56 |
| HMC-2 | 180.81 | 2.5 | 180.81 | 34.98 | 6.09 |
| HMC-3 | 158.77 | 5 | 158.77 | 25.82 | 7.05 |
| HMC-4 | 123.40 | 10 | 123.40 | 20.77 | 6.52 |

Notes: $\sigma_c$ is the peak strength, $E_s$ is elastic modulus, and $\varepsilon_{1c}$ is the strain at peak strength.

for each stage of the multistage creep test could be determined according to the triaxial compression strength as shown in Table 3.

Based on the testing system aforementioned, the triaxial creep test and permeability test on sandstone under HM coupling conditions are performed in the following steps (Figure 5).

(1) Install the rock sample and other devices, sealed the triaxial cell, and then rise the confining pressure to 5 MPa at the loading rate of 3 MPa/min

(2) Increase the pore pressure to the predetermined value (0, 2.5, 5.0, and 10.0 MPa) at the both ends of the rock sample and maintained it for 1 h so that the water pressure can completely penetrate the sandstone sample. After that, test the initial permeability ($k_0$) of red sandstone before creep test

(3) Increase the pore pressure to the predetermined value (0, 2.5, 5.0, and 10.0 MPa) at the both ends of the rock sample and maintained it

(4) Apply the axial load to predetermined value (i.e., 80 MPa/0.4$\sigma_c$) of the first stage on the rock sample at the rate of 30 MPa/min, then test the permeability ($k_1$) of sandstone sample. After that, keep deviatoric stress constant for 8 hours. During the first stage creep, the permeability was tested every 2 hours ($k_2 \sim k_5$). Increase the axial load to next stage and repeat the operations after 8 hours

(5) Stop the creep test when the red sandstone sample is fractured, maintain the confining pressure, and test the permeability of fractured sandstone ($k_f$).

The transient pulse method has been widely adopted to measure the permeability of sandstone in this test [24–26]. In a single permeability test, firstly, we adjust the hydraulic pore pressure upstream to 1.5 MPa and hydraulic pore pressure downstream to 0.5 MPa. Therefore, the hydraulic pressure difference is determined at 1.0 MPa between the upstream and the downstream at the beginning. The rock permeability is calculated according to Darcy Equation (1) [27]. All tests were conducted at room temperature.

$$k = \mu_w \beta V \frac{\ln\left(\Delta P_0 / \Delta P_t\right)}{2t\left(A_s / L_s\right)}, \tag{1}$$

where $\mu_w$ is the viscosity coefficient of water ($\mu_g = 1 \times 10^{-3}$ Pa · s), $\beta$ is the compressibility of water ($\beta = 4.53 \times 10^{-10}$ Pa$^{-1}$), $L_s$ is the length of the rock specimen (m), $A_s$ is the cross-sectional area of the rock specimen (m$^2$), $V_u$ is the volume of water tank (473 cm$^3$), $\Delta P_0$ and $\Delta P_t$ indicate the hydraulic pressure differences of the upstream and

Table 3: Stress for each stage in multistage creep test (MPa).

| Specimen | 1 | 2 | 3r | 4th | 5 | 6 |
|---|---|---|---|---|---|---|
| HML-1~4 | 80 ($0.4\sigma_c$) | 100 ($0.5\sigma_c$) | 120 ($0.6\sigma_c$) | 140 ($0.7\sigma_c$) | 160 ($0.8\sigma_c$) | 180 ($0.9\sigma_c$) |

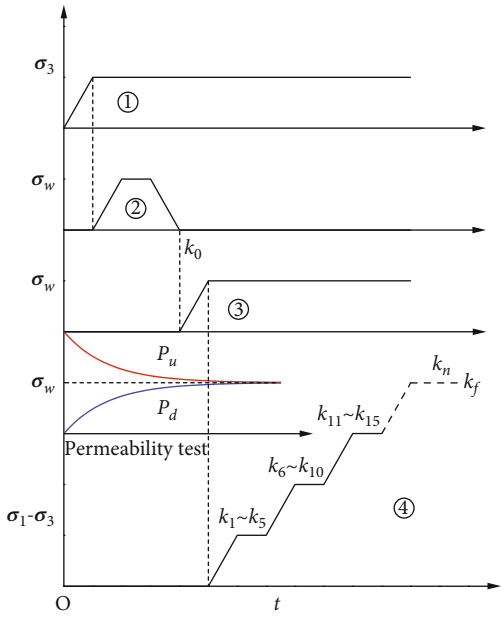


Figure 5: Testing procedure.

downstream at the beginning and time $t$ (MPa), and $t$ is the duration of the permeability test (s).

## 3. Experimental Results

*3.1. Creep Strain Behavior.* Figure 6 shows the creep strain-time curves of red sandstone under different pore pressures. It is noted that the strain-time curves of all samples could be divided into three stages, i.e., decelerating creep stage, steady-state creep stage, and accelerating creep stage [10, 14]. For sandstone samples under different pore pressures, the creep behavior is different. The larger the pore pressure is, the shorter the creep time of sandstone is. At $\sigma_w = 0$ MPa, the sandstone sample fractured at the 5th creep stage load ($\sigma_1 - \sigma_3 = 40$ MPa), and the duration of total creep test lasted 36.13 h. With the increase in pore pressure, the duration of the creep test gradually decreases. At $\sigma_w = 2.5$ MPa, red sandstone fractured immediately the 5th stage stress was applied. Other samples were destroyed at the 4th and 3rd stages, and the creep test durations are 29.09d and 22.17d, respectively. In addition, the creep strain of sandstone samples also increases with the increase in pore pressure. Taking the first stage creep loading as an example, the axial strain of sandstone reaches 0.14%, 0.16%, 0.22%, and 0.33% at the end of the first stage, respectively.

*3.2. Creep Deformation.* During creep test, the deformation of rock could be divided into instantaneous deformation and creep deformation. Figure 7 shows the relationships between instantaneous strain and creep strain with stress ratio ($r_\sigma$) under different pore pressures. It is observed that both instantaneous strain and creep strain of sandstone increase with the increase in deviatoric stress. At $\sigma_w = 0$ MPa and $r_\sigma = 0.4$, the instantaneous strain and creep strain of sandstone are 0.096% and 0.12%, respectively; when sandstone samples were fractured ($r_\sigma = 0.8$), the instantaneous strain and creep strain of the sample increase by 2.30 times and 6.81 times, respectively, compared to those under the first stage load. The fitting results of instantaneous strain, creep strain, and stress ratio are also plotted in Figure 7. The relationship between instantaneous strain and stress ratio is linear positive correlation, and that between creep strain and stress ratio is exponential positive function.

*3.3. Permeability Evolution.* The stress-strain and permeability-strain curves of red sandstone samples under triaxial multistage creep show that the permeability of rock decreases first but then increases with the increase in creep tome and axial load (Figure 8). Figure 9 demonstrates that the intact red sandstone samples are low-permeable rock as the permeability of saturated samples before creep test is below $10^{-15}$ m$^2$. A small decrease in rock permeability occurs, as the axial load was rose to the first stage load, indicating that the initial voids in sandstone samples are compacted. The permeability remains relatively constant during the steady creep stage. However, there is a slight increase in rock permeability with the increase in the axial load at the beginning of each stage. There is significant increase in rock permeability after the sample is fractured; the permeability $k_f$ is 3.10, 2.62, 1.52, and 1.50 times larger than the last permeability during creep test.

Basically, all permeability-time curves show a "decreasing-steady-increasing" trend. However, it should be noted that there are two different permeability evolution trends during the steady creep stage. The first trend is that the permeability gradually increases with the increase in axial strain, while the second trend shows the opposite, i.e., the permeability decreases with the increasing axial strain. Considering the deviatoric stress, it is observed that the permeability tends to decrease under small deviatoric stress but turns to increase under large deviatoric stress.

## 4. Discussion

*4.1. Determination of Long-Term Strength.* The isochronous stress-strain curve method is the most commonly used method to determine the long-term strength of rock. According to the creep curve, the isochronous stress-strain curves can be obtained by selecting the stress and strain at a certain time. Therefore, the isochronous stress-strain curve cluster is formed based on several isochronous stress-strain curves. The isochronous stress-strain curve method regarded the stress corresponding to inflexion point on the isochronous

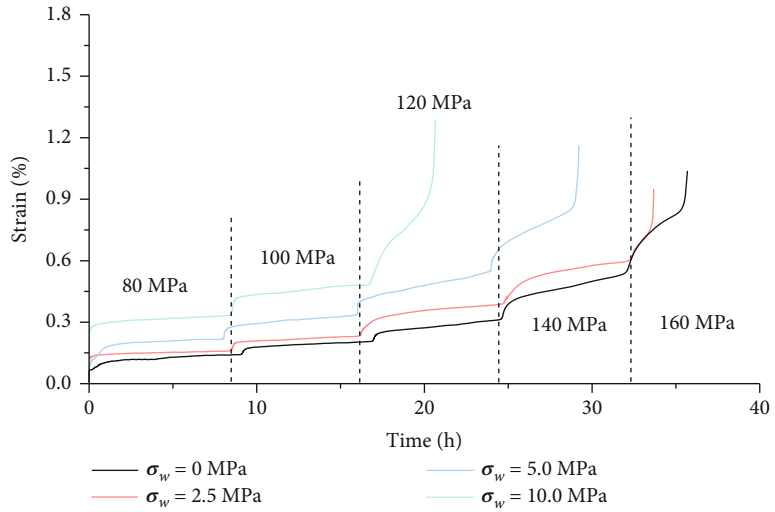


Figure 6: Creep curves of sandstone under different water pressures.

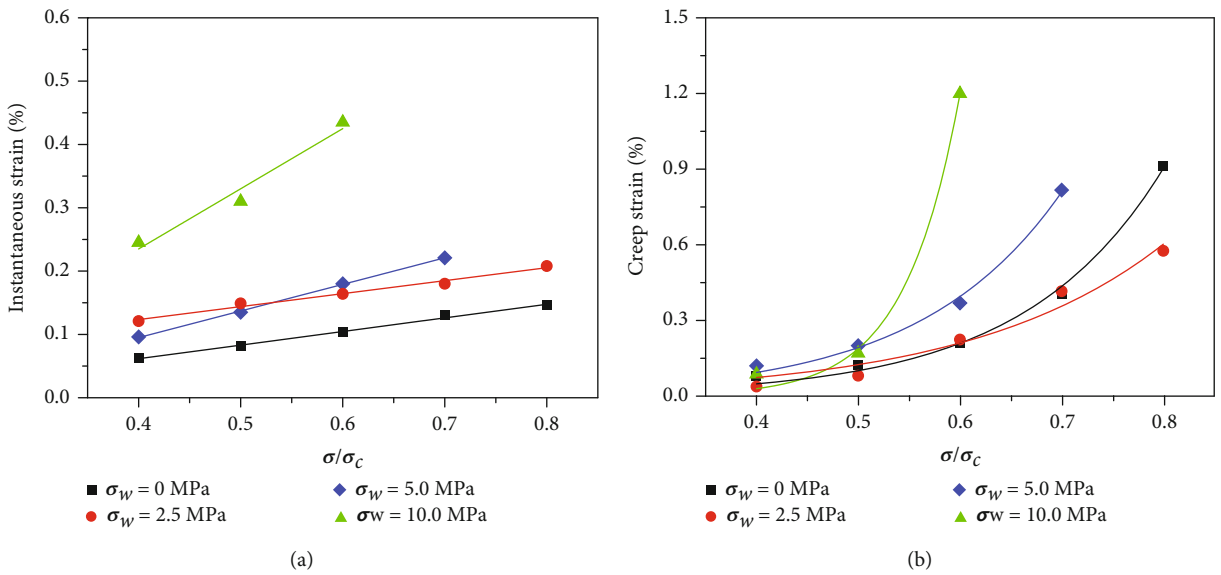


Figure 7: Creep deformation curves of sandstone under different conditions. (a) Instantaneous strain and (b) creep strain.

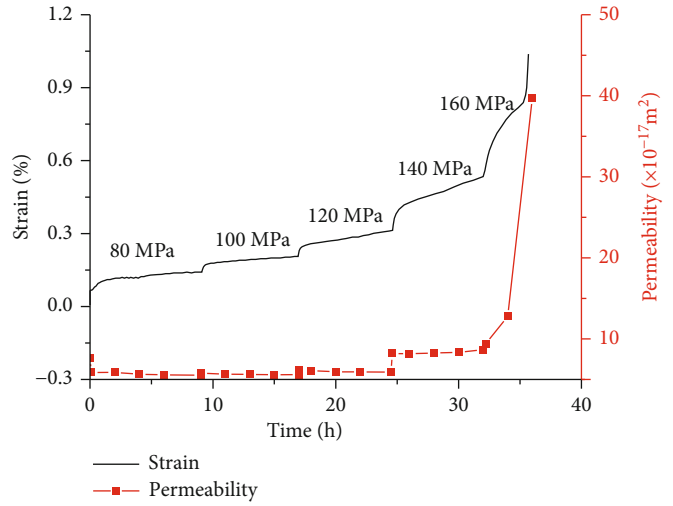


(a)

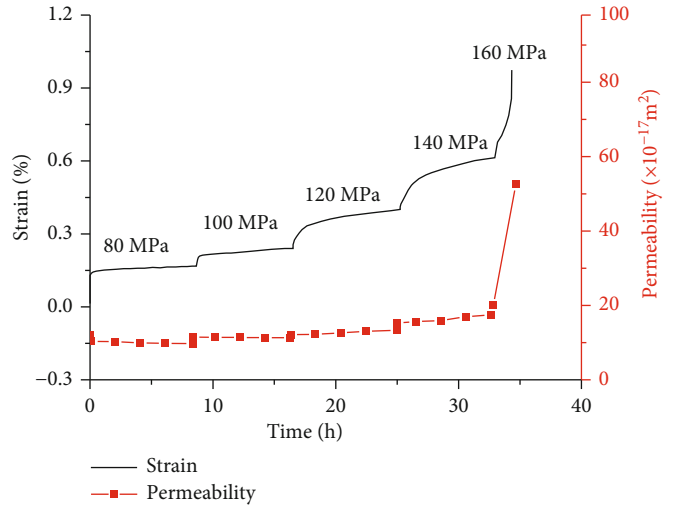


(b)

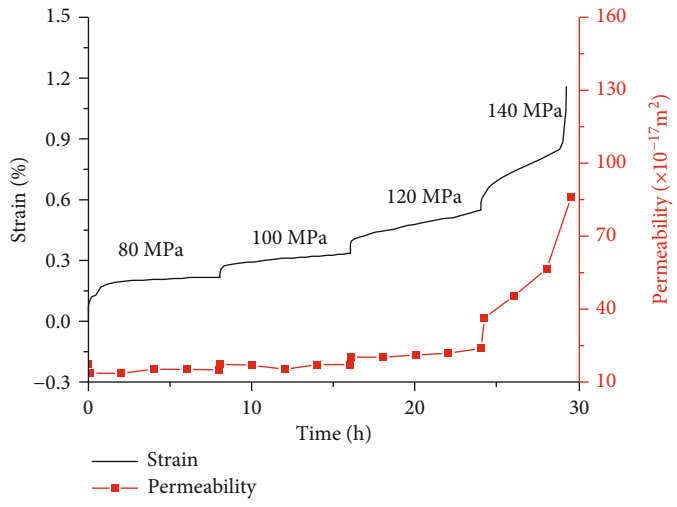


(c)

Figure 8: Continued.

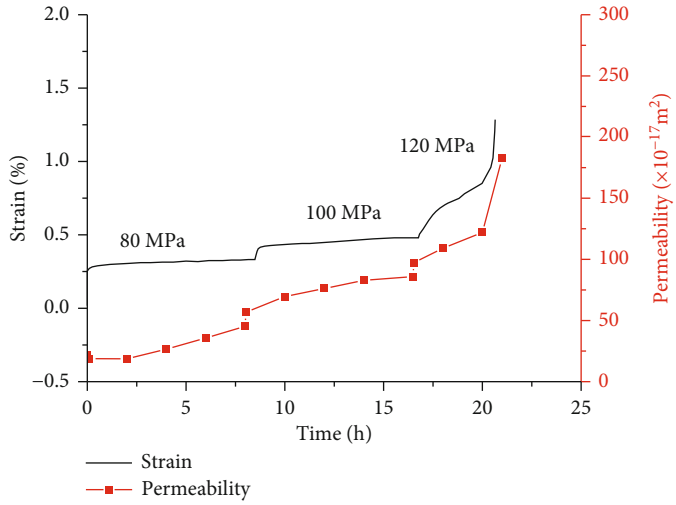


(d)

Figure 8: Permeability and strain evolution with time of sandstone under different water pressures. (a) $\sigma_w = 0$ MPa, (b) $\sigma_w = 2.5$ MPa, (c) $\sigma_w = 5.0$ MPa, and (d) $\sigma_w = 10.0$ MPa.

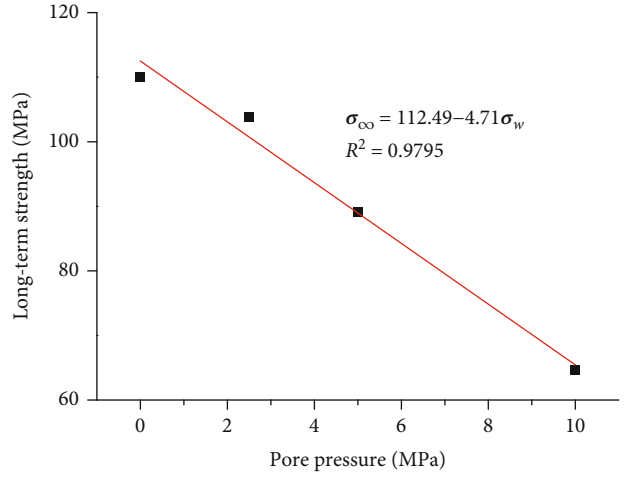


Figure 9: Relationship between long-term strength of sandstone and pore pressure.

stress-strain curve cluster as the long-term strength of rock as shown in Figure 10 [28, 29].

Constant load creep test and multistage creep test are usually used to determine the long-term mechanical properties of rock. However, constant load creep test is time-consuming and expensive, thus making multistage creep test more popular. Since some factors, for instance, temperature, pore pressure, and water content, have obvious weakening effect on the mechanical properties of rock, the rock sample may have fractured under the first or second stage of creep test. In this case, it is hard to determine the long-term strength of rock samples based on the isochronous stress-strain curve method. Figure 11 shows the isochronous stress-strain curves of red sandstone samples in this experiment, and it is noted that the long-term strength of tested sandstone is 118.24 MPa and 104.35 MPa at $\sigma_w = 0$ MPa and $\sigma_w = 2.5$ MPa. However, at $\sigma_w = 5.0$ MPa and $\sigma_w = 10.0$ MPa, samples were fractured at the third or the fourth stage; therefore, we could not determine the inflection point on isochronous stress-strain curves.

Typical stress-strain curves and characteristic stress of brittle rock are shown in Figure 12. Martin et al. [30] proposed a method for determining the long-term strength of rock based on the volume dilatancy characteristics. This method uses the inflection point of deviatoric stress-volume strain curve in conventional triaxial stress-strain curve of rock to determine the long-term strength of rock. According to this method, the long-term strength of sandstone under different pore pressures is 130.04 MPa, 123.91 MPa, 109.07 MPa, and 81.56 MPa, respectively. Ding et al. [31] put forward another method to determine the long-term strength of salt rock which is based on the crack initiation point, i.e., they proposed that $\sigma_{ci}$ represented the long-term strength of salt rock. Based on these investigations, we compared the results obtained by different long-term strength determining methods (Table 4). It is noted that the long-term strength of red sandstone obtained by isochronous stress-strain curve method and $\sigma_{ci}$ are very close under the pore pressure of 0 MPa and 2.5 MPa, while $\sigma_\infty$ determined by $\sigma_{cd}$ is much higher than the other two methods. Therefore, it can be known that the long-term strength of rock can be obtained based on $\sigma_{ci}$, which are 112.15 MPa, 103.21 MPa, 89.87 MPa, and 64.78 MPa, respectively. Figure 9 shows the long-term strength evolution with pore pressure; it is observed that the long-term strength of red sandstone gradually decreases with the increase in pore pressure, and there is a linear negative correlation between them.

*4.2. Permeability and Pore Pressure.* Based on the permeability-time curves of sandstone at different pore pressures, permeability of intact and fractured red sandstone samples is obtained, and the permeability evolution with pore pressure curves is plotted in Figure 13. For a given confining pressure, the permeability of both intact and fractured

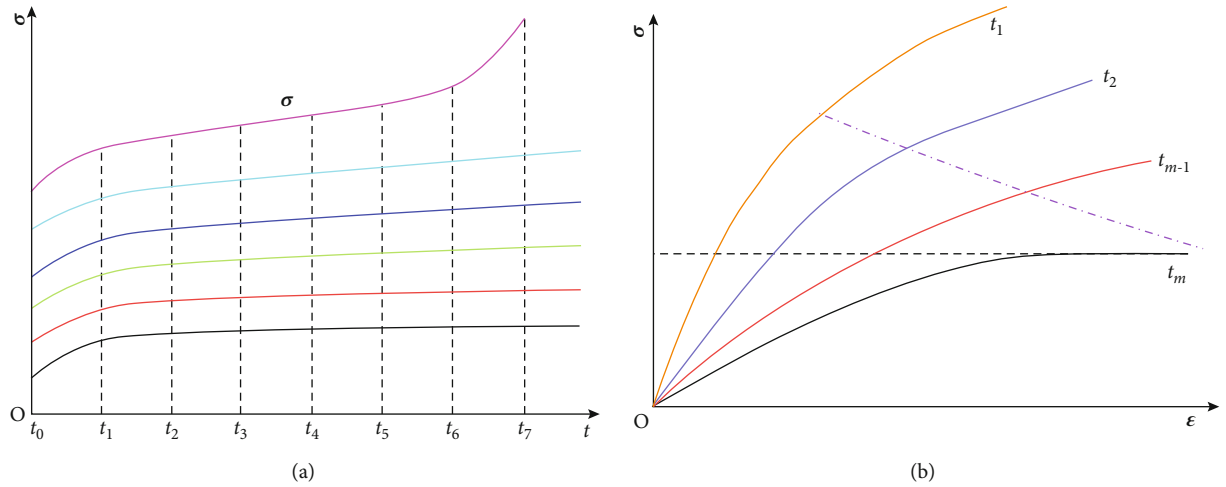


Figure 10: Isochronous stress-strain curve method. (a) Graded creep curve and (b) isochronous stress-strain curves.

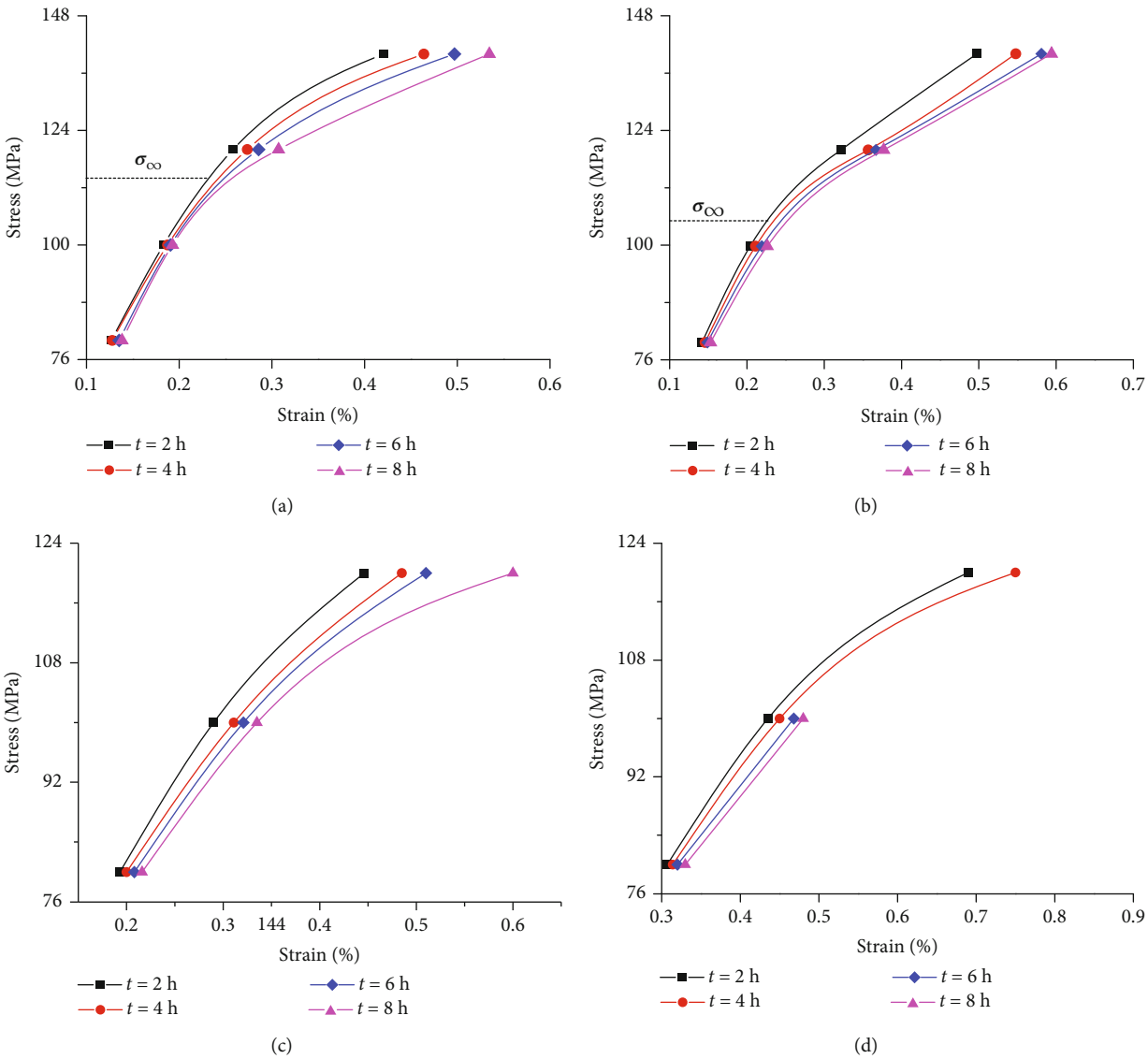


Figure 11: Long-term strength of sandstone based on isochronous stress-strain curve method. (a) $\sigma_w$ = 0 MPa, (b) $\sigma_w$ = 2.5 MPa, (c) $\sigma_w$ = 5.0 MPa, and (d) $\sigma_w$ = 10.0 MPa.

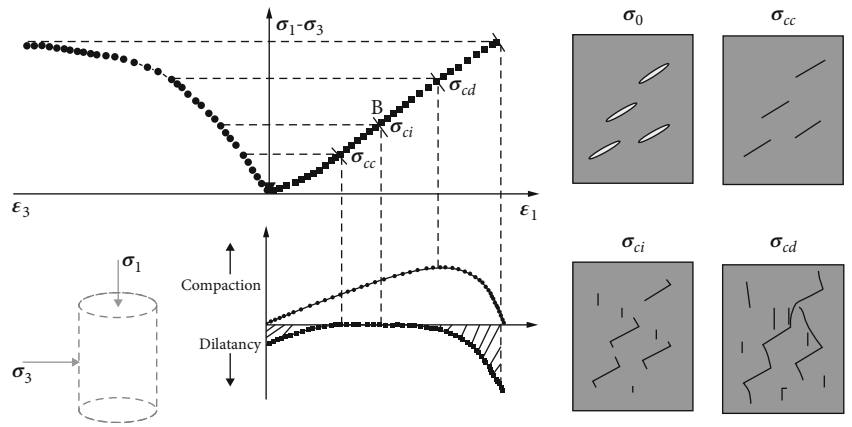


Figure 12: Typical stress-strain curves of brittle rock.

Table 4: Long-term strength ($\sigma_\infty$) of sandstone under different hydraulic pressures (MPa).

| Determining method | $\sigma_w$ = 0 MPa | $\sigma_w$ = 0.5 MPa | $\sigma_w$ = 1.0 MPa | $\sigma_w$ = 2.0 MPa |
|---|---|---|---|---|
| Isochronous stress-strain curve method | 118.24 | 104.35 | / | / |
| Volume dilatancy method | 130.04 | 123.91 | 109.07 | 81.56 |
| Crack initiation method | 112.15 | 103.21 | 89.87 | 64.78 |

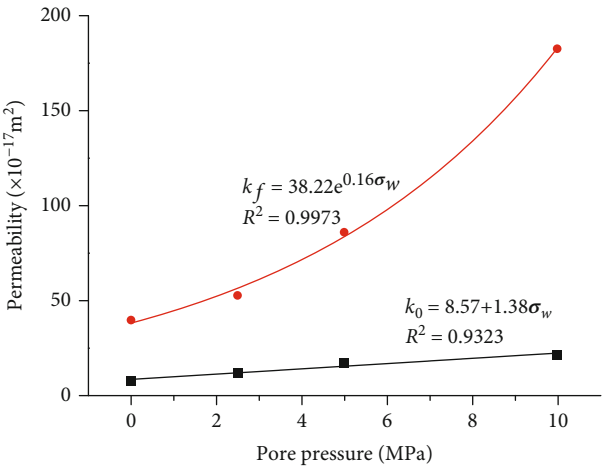


Figure 13: Permeability of intact and fractured red sandstone samples evolution with pore pressure.

Figure 14: Failure mode of fractured red sandstone samples after the triaxial creep test.

sandstone samples increases with the increase in pore pressure. However, it should be noted that the relationship between $k_0$ and $\sigma_w$ is positive linear, while it is a positive exponential function between $k_f$ and $\sigma_w$.

Figure 14 shows the fractured red sandstone samples after the triaxial creep test. It is noted that the failure mode of samples at different pore pressures is different. At $\sigma_w = 0$ MPa and 2.5 MPa, the specimen indicated a typical shear failure mode with a single fracture surface. At $\sigma_w = 5$ MPa, the failure mode of red sandstone specimen is complicated. It is noted that multishear fracture surfaces were formed during creep test, and tensile cracks are also observed on the specimen. However, for the red sandstone specimen at $\sigma_w = 10$ MPa, the rock sample is fragmented into four parts with X-shaped conjugate slopes. It should also be noted that the lateral deformation of red sandstone specimen is much larger than that of the other samples. The larger the pore pressure is, the greater the rock fragmented. This explains why the permeability of fractured sandstone samples increases with the increase in pore pressure (Figure 8).

## 5. Conclusion

To investigate the effects of pore pressure on the long-term mechanical properties and permeability evolution characteristics of red sandstone, the triaxial creep test and permeability on sandstone under different hydraulic pressures were conducted using MTS 815 testing system. The main conclusions are as follows:

(1) With the increase in pore pressure, the duration of creep test on red sandstone samples progressively decreases. The duration of creep test under different

pore pressures is 36.13d, 34.02d, 29.09d, and 22.17d, respectively

(2) Water effect significantly decreases the long-term strength of red sandstone samples. The long-term strength of sandstone at $\sigma_w = 0$ MPa is 110.35 MPa, and it decreases by 4.74%, 16.18%, and 32.67%, respectively, at other pore pressures, indicating a linear negative relationship

(3) For a given confining pressure, the permeability of both intact and fractured sandstone samples increases with the increase in pore pressure. However, it should be noted that the relationship between $k_0$ and $\sigma_w$ is positive linear, while it is a positive exponential function between $k_f$ and $\sigma_w$

(4) The larger the pore pressure is, the greater the rock fragmented. The failure mode of red sandstone samples gradually becomes more complex, which transforms from typical shear failure to shear failure of multiple shear planes

## Data Availability

All data are available on request.

## Conflicts of Interest

The author declares no conflict of interests related to this article.

## Acknowledgments

The author would like to express his gratitude to NSFC for the financial support by approving the project (Grant No. 51808203).

## References

[1] X. Cheng, W. Xu, C. Yue, X. Du, and C. H. Dowding, "Seismic response of fluid–structure interaction of undersea tunnel during bidirectional earthquake," *Ocean Engineering*, vol. 75, pp. 64–70, 2014.

[2] Z. D. Eisenstein, "Large undersea tunnels and the progress of tunnelling technology," *Tunnelling and Underground Space Technology*, vol. 9, no. 3, pp. 283–292, 1994.

[3] S. Li, H. Liu, L. Li, Q. Zhang, K. Wang, and K. Wang, "Large scale three-dimensional seepage analysis model test and numerical simulation research on undersea tunnel," *Applied Ocean research*, vol. 59, pp. 510–520, 2016.

[4] M. Ikuma, "Maintenance of the undersea section of the Seikan Tunnel," *Tunnelling and Underground Space Technology*, vol. 20, no. 2, pp. 143–149, 2005.

[5] S. P. Dutton, W. A. Flanders, and M. D. Barton, "Reservoir characterization of a Permian deep-water sandstone, East Ford field, Delaware basin, Texas," *AAPG Bulletin*, vol. 87, no. 4, pp. 609–627, 2003.

[6] P. Baud, W. Zhu, and T. F. Wong, "Failure mode and weakening effect of water on sandstone," *Journal of Geophysical Research: Solid Earth*, vol. 105, no. B7, pp. 16371–16389, 2000.

[7] H. Yang and X. Deng, "Deposition of Yanchang Formation deep-water sandstone under the control of tectonic events in the Ordos Basin," *Petroleum Exploration and Development*, vol. 40, no. 5, pp. 549–557, 2013.

[8] Z. Li, S. Liu, W. Ren, J. Fang, Q. Zhu, and Z. Dun, "Multiscale laboratory study and numerical analysis of water-weakening effect on shale," *Advances in Materials Science and Engineering*, vol. 2020, Article ID 5263431, 14 pages, 2020.

[9] C. Zhu, X. Xu, X. Wang et al., "Experimental investigation on nonlinear flow anisotropy behavior in fracture media," *Geofluids*, vol. 2019, Article ID 5874849, 9 pages, 2019.

[10] X. Zhang, Y. Wu, E. Zhai, and P. Ye, "Coupling analysis of the heat-water dynamics and frozen depth in a seasonally frozen zone," *Journal of Hydrology*, vol. 593, no. article 125603, 2020.

[11] C. Zhu, M. He, M. Karakus, X. Cui, and Z. Tao, "Investigating toppling failure mechanism of anti-dip layered slope due to excavation by physical modelling," *Rock Mechanics and Rock Engineering*, vol. 53, no. 11, pp. 5029–5050, 2020.

[12] Z. Li, H. Zhou, D. Hu, and C. Zhang, "Yield criterion for rock-like geomaterials based on strain energy and CMP model," *International Journal of Geomechanics*, vol. 20, no. 3, article 04020013, 2020.

[13] C. Zhu, K. Zhang, H. Cai et al., "Combined application of optical fibers and CRLD bolts to monitor deformation of a pit-in-pit foundation," *Advances in Civil Engineering*, vol. 2019, Article ID 2572034, 16 pages, 2019.

[14] Q. Meng, H. Wang, M. Cai, W. Xu, X. Zhuang, and T. Rabczuk, "Three-dimensional mesoscale computational modeling of soil-rock mixtures with concave particles," *Engineering Geology*, vol. 277, article 105802, 2020.

[15] Z. Li, H. Liu, Z. Dun, L. Ren, and J. Fang, "Grouting effect on rock fracture using shear and seepage assessment," *Construction and Building Materials*, vol. 242, article 118131, 2020.

[16] H. Liu, W. Zhu, Y. Yu, T. Xu, R. Li, and X. Liu, "Effect of water imbibition on uniaxial compression strength of sandstone," *International Journal of Rock Mechanics and Mining Sciences*, vol. 127, article 104200, 2020.

[17] B. Vásárhelyi and P. Ván, "Influence of water content on the strength of rock," *Engineering Geology*, vol. 84, no. 1-2, pp. 70–74, 2006.

[18] D. Li, L. N. Y. Wong, G. Liu, and X. Zhang, "Influence of water content and anisotropy on the strength and deformability of low porosity meta-sedimentary rocks under triaxial compression," *Engineering Geology*, vol. 126, pp. 46–66, 2012.

[19] G. Chen, T. Li, W. Wang, Z. Zhu, Z. Chen, and O. Tang, "Weakening effects of the presence of water on the brittleness of hard sandstone," *Bulletin of Engineering Geology and the Environment*, vol. 78, no. 3, pp. 1471–1483, 2019.

[20] C. Yu, S. Tang, C.'. Tang et al., "The effect of water on the creep behavior of red sandstone," *Engineering Geology*, vol. 253, pp. 64–74, 2019.

[21] S. B. Tang, C. Y. Yu, M. J. Heap, P. Z. Chen, and Y. G. Ren, "The influence of water saturation on the short- and long-term mechanical behavior of red sandstone," *Rock Mechanics and Rock Engineering*, vol. 51, no. 9, pp. 2669–2687, 2018.

[22] S.-Q. Yang, H.-W. Jing, and L. Cheng, "Influences of pore pressure on short-term and creep mechanical behavior of red sandstone," *Engineering Geology*, vol. 179, pp. 10–23, 2014.

[23] R. Ulusay and J. Hudson, *The Complete ISRM Suggested Methods for Rock Characterization, Testing and Monitoring*, ISRM Turkish National Group, Ankara, Turkey, 2007.

[24] F. Fedor, G. Hámos, A. Jobbik, Z. Máthé, G. Somodi, and I. Szűcs, "Laboratory pressure pulse decay permeability measurement of Boda Claystone, Mecsek Mts., SW Hungary," *Physics and Chemistry of the Earth, Parts A/B/C*, vol. 33, pp. S45–S53, 2008.

[25] Q. Zhang, J. Liu, H. Xu, Y. Zeng, C. Wang, and L. Wang, "Experimental investigation on permeability evolution of limestone caprock under coupled THM processes," *KSCE Journal of Civil Engineering*, vol. 23, no. 12, pp. 5090–5097, 2019.

[26] Q. Liu, K. Zhang, H. Zhou, Y. Cheng, H. Zhang, and L. Wang, "Experimental investigation into the damage-induced permeability and deformation relationship of tectonically deformed coal from Huainan coalfield, China," *Journal of Natural Gas Science and Engineering*, vol. 60, pp. 202–213, 2018.

[27] W. F. Brace, J. B. Walsh, and W. T. Frangos, "Permeability of granite under high pressure," *Journal of Geophysical Research*, vol. 73, no. 6, pp. 2225–2236, 1968.

[28] C. Liu, J. Zhang, M. Zhang, and F. Zhang, "Experimental study of short-term creep characteristics base on step loading-unloading method for hard rock," *Journal of Experimental Mechanics*, vol. 5, pp. 86–93, 2009.

[29] F. Wu, H. Zhang, Q. Zou, C. Li, J. Chen, and R. Gao, "Visco-elastic-plastic damage creep model for salt rock based on fractional derivative theory," *Mechanics of Materials*, vol. 150, article 103600, 2020.

[30] C. D. Martin and N. A. Chandler, "The progressive fracture of Lac du Bonnet granite," *International Journal of Rock Mechanics and Mining Sciences & Geomechanics Abstracts*, vol. 31, no. 6, pp. 643–659, 1994.

[31] G. Ding, J. Liu, L. Wang, Z. Wu, and Z. Zhou, "Discussion on determination method of long-term strength of rock salt," *Energies*, vol. 13, no. 10, p. 2460, 2020.